October 2017
Volume 15, Number 4

THE Ocular Surface

A JOURNAL OF REVIEW LINKING LABORATORY SCIENCE, CLINICAL SCIENCE, AND CLINICAL PRACTICE
A peer-reviewed quarterly journal

Indexed in MEDLINE/PubMed and EMBASE

Editorial

INTERESTS

J. Daniel Nelson, MD, FACS, FARVO

Clinical Science

REVIEW: THE FUNCTION OF REGULATORY T CELLS AT THE OCULAR SURFACE

William Foulsham, Anna Marmalidou, Afsaneh Amouzegar, Giulia Coco, Yihe Chen, and Reza Dana

Foxp3+ Tregs are critical to immune homeostasis and the prevention of autoimmunity and chronic inflammation. Potentially, Treg immunotherapy at the ocular surface could be effective, particularly in the setting of autoimmune disease and high-risk corneal transplantation.

REVIEW: MICRORNAS IN OCULAR SURFACE AND DRY EYE DISEASES

Diane Meyre Rassi, Cintia S. de Paiva, Lara Cristina Dias, Carolina Maria Módulo, Leidiane Adriano, Marina Zilio Fantucci, and Eduardo Melani Rocha

This review describes the current understanding of miRNAs as biomarkers, mediators of diseases, and potential therapeutic targets in ocular surface diseases.

REVIEW: EMERGING STRATEGIES FOR ANTIMICROBIAL DRUG DELIVERY TO THE OCULAR SURFACE: IMPLICATIONS FOR INFECTIOUS KERATITIS

Ajay Sharma, and Jonathan Taniguchi

Drug delivery systems that can enhance penetration and extend the duration of antimicrobial presence on the ocular surface are being developed. Results of tests in in vitro models, ex vivo excised corneas, and in vivo rabbits are reviewed.

REVIEW: ENVIRONMENTAL IMPACT ON OCULAR SURFACE DISORDERS: POSSIBLE EPIGENETIC MECHANISM MODULATION AND POTENTIAL BIOMARKERS

Anna Busanello, PhD, Daniela Santucci, PhD, Stefano Bonini, MD, and Alessandra Micera, PhD

Physical and chemical stressors at the ocular surface might influence normal microbiota and contribute to local disorders. Epigenetic modulation could potentially enhance the treatment of ocular surface diseases.

Innovative Techniques and Technology

ROLE OF HIGH RESOLUTION OPTICAL COHERENCE TOMOGRAPHY IN DIAGNOSING OCULAR SURFACE SQUAMOUS NEOPLASIA WITH COEXISTING OCULAR SURFACE DISEASES

Marwan Atallah, MD, Madhura Joag, MD, Anat Galor, MD, MSPH, Guillermo Amescua, MD, Afshan Nanji, MD, MPH, Jianhua Wang, MD, PhD, Victor L. Perez, MD, Sander Dubovy, MD, and Carol L. Karp, MD

While histopathology is the gold standard in the diagnosis of OSSN, HR-OCT can be used to noninvasively detect the presence of OSSN in patients with coexisting ocular conditions.

Original Research

A LINK BETWEEN TEAR BREAKUP AND SYMPTOMS OF OCULAR IRRITATION

Jun Zhang, Carolyn G. Begley, OD, MS, Ping Situ, PhD, Trefford Simpson, Dip Optom, MSc, PhD, and Haixia Liu, PhD

Our sustained tear exposure (STARE model) demonstrated that tear breakup was associated with increased discomfort, which was at least partially blocked by wearing a contact lens, suggesting ocular surface neural stimulation by adverse conditions within tear breakup.

MEIBOMIAN GLAND MORPHOGENESIS REQUIRES DEVELOPMENTAL EYELID CLOSURE AND LID FUSION

Jingjing Wang, PhD, Mindy Call, PhD, Maureen Mongan, BS, Winston Whei-Yang Kao, PhD, and Ying Xia, PhD

While Meibomian gland abnormalities were found in all eye-open-at-birth mice, the severity varied and corresponded to the position and the size of eye opening but not the genetic defects of the mice.

OCULAR SURFACE ALKALI INJURY DAMAGES MEIBOMIAN GLANDS IN MICE

Shin Mizoguchi, MD, PhD, Hiroki Iwanishi, MD, PhD, Masahide Kokado, MD, PhD, Takayoshi Sumioka, MD, PhD, Geraint J. Parfitt, PhD, Yilu Xie, PhD, Reiko Arita, MD, PhD, Rika Shirakawa, MD, PhD, Oyamu Yamanaka, MD, PhD, Yuka Okada, MD, PhD, James V. Jester, PhD, and Shizuya Saika, MD, PhD

Alkali injury to the ocular surface results in damage and destruction of the eyelid meibomian glands. The pattern of the tissue damage differs between glands of the upper and lower eyelids.

Contents Continued.....

tfos
Affiliated with the Tear Film & Ocular Surface Society

ELSEVIER

The Ocular Surface 15 (2017) 759–769

Contents lists available at ScienceDirect

The Ocular Surface

journal homepage: www.theocularsurface.com

Clinical and morphological manifestations of aniridia-associated keratopathy on anterior segment optical coherence tomography and in vivo confocal microscopy

Anna Voskresenskaya [a, *], Nadezhda Pozdeyeva [a, b], Tatyana Vasilyeva [c], Yevgeniy Batkov [a], Aleksandr Shipunov [a], Boris Gagloev [a], Rena Zinchenko [c, d]

[a] Cheboksary branch of S. Fyodorov Eye Microsurgery Federal State Institution, Cheboksary, Russian Federation
[b] Postgraduate Medical Institute, Cheboksary, Russian Federation
[c] Federal State Budgetary Institution, Research Center for Medical Genetics, Moscow, Russian Federation
[d] Pirogov Russian National Research Medical University, Moscow, Russian Federation

ARTICLE INFO

Article history:
Received 22 April 2017
Received in revised form
12 June 2017
Accepted 5 July 2017

Keywords:
Aniridia-associated keratopathy
Anterior segment optical coherence tomography
Laser scanning confocal microscopy
Palisades of Vogt
Congenital aniridia
Limbal stem cell deficiency

ABSTRACT

Purpose: The study aimed to evaluate clinical and morphological changes in the limbal palisades of Vogt (POV) at different stages of aniridia-associated keratopathy (AAK) and to assess possible utility of anterior segment optical coherence tomography (AS-OCT) for the visualization of limbal progenitor structures as it correlates to laser scanning confocal microscopy (LSCM) data.

Methods: The study involved 32 patients (59 eyes) with congenital aniridia. AAK stage was defined based on biomicroscopy. Assessment of limbal zone and detection of POVs in identical areas was performed by LSCM (HRT3) and AS-OCT (RTVue XR Avanti) using 3D Cornea (En Face mode) and Cornea Cross Line protocols.

Results: Intact and changed POVs were found in 8/8 stage 0 eyes, in 1/21 stage I and 2/13 stage II eyes. Spearman's correlation coefficient in assessing the consistency of the POV diagnostic results by LSCM and AS-OCT for the inferior limbus was $r_S = 0.85$ ($P < 0.05$), for the superior limbus – $r_S = 0.53$ ($P < 0.05$). AS-OCT was less sensitive for detection of partially present POVs in superior limbus. The negative correlation between AAK stage and POV preservation was determined ($r_S = -0.5$, $P < 0.05$). There was no correlation between AAK stage and patient age ($r_S = 0.235$, $P = 0.209$). Three patients with *PAX6* 3′ deletion showed stage 0 AAK with intact or slightly disturbed POVs morphology and transparent cornea.

Conclusion: AS-OCT may be an additional diagnostic tool for POV visualization in vivo in aniridic patients. Its diagnostic accuracy is subject to selection of anatomic region, nystagmus and the degree of POV degradation.

1. Introduction

Congenital aniridia (OMIM 106210) is a genetically determined panocular malformation which is characterized by partial or complete absence of the iris, foveal and optic nerve hypoplasia, keratopathy, lens opacities, glaucoma, and nystagmus [1]. The complex nature of developmental disorders is in 85–90% of cases a result of heterozygous mutations in *PAX6* gene [2]. The global prevalence of this disease is 1:40 000–100 000 [3,4]. Aniridic patients suffer from progressive visual loss due to cataract, glaucoma, and keratopathy.

Aniridia-associated keratopathy (AAK) occurs in 20–90% of patients with aniridia [5,6]. Its pathogenesis is thought to be associated with primary limbal stem cell deficiency (LSCD) and alterations in limbal microenvironment due to a *PAX6* gene mutation. Currently there is sound scientific evidence for the active role of *PAX6* in extracellular matrix metabolism, normal expression of cytoskeleton protein, and cell adhesion molecules in the cornea [7,8]. According to Ramaesh et al., in 78% of cases the basis of AAK pathogenesis is the destruction of limbal microenvironment leading to abnormal reparative response, disruption of corneal epithelial cell migration and differentiation [9].

* Corresponding author. Cheboksary branch of S. Fyodorov Eye Microsurgery Federal State Institution, Tractorostroiteley St. 10, Cheboksary, 428028, Russian Federation.
E-mail address: vsolaris@mail.ru (A. Voskresenskaya).

http://dx.doi.org/10.1016/j.jtos.2017.07.001
1542-0124/

Besides, functional limbal stem cells (LSC) preserve corneal transparency and maintain its regenerative capacity. Experimental studies have decisively localized LCSs to the limbal crypts and focal stromal projections (FSP) of the cornea [10,11]. These structures represent a clinical marker of LCS [12] and their absence due either to chemical/thermal burns or genetic defect (congenital aniridia) indicates development of LSCD [11,13]. In the absence of diagnostic tools that are capable of explicit imaging of LSCs in vivo, palisades of Vogt (POV) and FSP serve as a justifiable proxy giving a general idea of the location and health of epithelial progenitor structures. The gold standard for visualization of corneal morphological changes in vivo is corneal confocal microscopy. Evaluation of corneal epithelial progenitor structures of the limbus is necessary for predicting future progression of AAK as well as tolerability of surgical interventions and visual prognosis in general. However, given the fragility of corneal epithelium in AAK, the need for topical anesthesia, and the labor- and time-intensive nature of laser scanning confocal microscopy (LSCM) of the limbal area, it would be useful to assess the diagnostic value and clinical utility of alternative tools for visualizing the corneal epithelial progenitor structures.

Based on the above considerations, the purpose of the study was to investigate morphological changes in POV at various AAK stages and assess the ability to effectively visualize limbal progenitor structures in patients with aniridia using anterior segment optical coherence tomography (AS-OCT) as it correlates to LSCM data.

2. Material and methods

2.1. Patients

The study was performed in accordance with the principles of the Declaration of Helsinki. All patients reviewed and signed an informed consent for diagnostic examination and possible consequences of the procedure. Ethics approval was obtained from the local Ethics Committee of the Postgraduate Medical Institute (Cheboksary, Russia). All patients attended Cheboksary branch of S. Fyodorov Eye Microsurgery Federal State Institution and were recruited from June 2015 to August 2016.

Thirty two patients (59 eyes) with congenital aniridia were examined, including 16 women and 16 men. Familial inheritance was noted in 22 persons with sporadic cases of aniridia being observed in 10 patients. The mean age was 32.5 ± 13 years (range, 4–56 years). In genetic analysis previously performed at the Federal State Budgetary Institution «Research Center for Medical Genetics» (Moscow), the causal mutation was found in 29 patients; in two cases, a *PAX6* mutation was not found by DNA-testing, which includes initial Sanger sequencing analysis followed by multiplex ligation-dependent probe amplification (MLPA). Genetic testing was not performed in 1 patient.

In addition to genetic testing, the diagnosis of congenital aniridia was based on clinical manifestation. The clinical presentation in aniridia patients comprised bilateral complete or partial aniridia, foveal hypoplasia, and sensory deficient congenital nystagmus. Other associated ocular features included AAK, cataract, and glaucoma. Biomicroscopy data served as the basis for scoring the severity of AAK. The classification scheme proposed by Eden et al. was used [14]. Superior and inferior limbi were imaged by AS-OCT and LSCM, considering predominantly localization of POVs in these quadrants in healthy subjects [11,15–18]. Given the non-invasive nature of AS-OCT, it was always done first, followed by LSCM, usually on the same diagnostic day.

2.2. Anterior segment optical coherence tomography

Limbal structures were imaged by AS-OCT (RTVue XR Avanti, Optovue, USA, software version 2016.1.0.26) with a cornea anterior module long adapter lens. For POV visualization, a 3D Cornea protocol in En Face mode was applied. Scanning zone dimensions for 3D Cornea protocol were 4*4 and 4*6 mm with axial resolution of 5 μm. In all patients, scanning was performed in the superior and inferior limbal sectors within an arc length of 90°. In order to visualize POVs in proper quality, a standard scanning layer thickness of 30 μm was used (En Face mode). To look for progenitor structure changes, the depth position of the scan line was adjusted to obtain the sharpest image. The acquired images were analyzed for the presence of POVs with attention to their structural features and visibility. The Cornea Cross Line protocol was used to determine the location of palisades relative to the surface.

2.3. Laser scanning confocal microscopy

Detailed examination of the central corneal zone, limbal POV/FSP structures, and limbal/corneal transition areas, and detection of inflammatory changes in the superior and inferior limbus was performed on Heidelberg Retina Tomograph (HRT3) with Rostock Cornea Module (Heidelberg Engineering, Germany). Images were acquired in the sequence scan mode at a rate of 30 frames/sec. Assessment of POV was conducted in the superior and inferior limbal sectors within 90°. First, the operator visualized basal epithelium in the central cornea followed by a shift to the superior or inferior limbus at extreme abduction of the patient's gaze along the vertical meridian. The image size was 400 × 400 μm, the optical section depth was 4 μm. A single operator examined all the patients. LSCM was used as a control and a basic limbal POV detection method.

We judged the presence of limbal basal cells with dark cytoplasm and distinct light borders, POV structures in the form of hyper-reflective double-contoured usually parallel trabecular extensions with an internal acellular region and FSP in the form of double-contoured oval or circular structures as morphological criteria for the integrity of progenitor structures in the limbal zone [15,19]. In the absence of distinctly visible intact progenitor zones, the images were assessed for the presence of detectable palisade-like structures or partially present POVs. They were defined as recognizable by morphology, but incomplete or abnormal in appearance [19]. Distorted POVs appeared as indistinct horizontal ridge-like structures and stubs, short shallow palisade ridge remnants without double contour and FSP with reduced reflectivity. Absence of limbal progenitor structures was determined, when neither palisade-like structures, nor FSPs were detected in the entire study region.

2.4. Statistical analysis

The analysis was performed using STATISTICA software (StatSoft Inc., version 6.1). The Mann-Whitney *U* test reserved for non-normally distributed data. The values of $P < 0.05$ were considered statistically significant. Correlation analysis of direct (LSCM) and indirect (AS-OCT) imaging of POVs was conducted using Spearman's rank correlation coefficient. The following ranks were assigned for this non-parametric test: 0 – no palisades, 1 – distorted palisades or palisade-like structures, 2 – normal appearing palisades. To correct for bilateral data dependency only one eye of every study subject was randomly selected for the data analysis.

3. Results

Demographic characteristics, genetic analysis data, keratopathy stage, LSCM and AS-OCT imaging results of patients with aniridia are summarized in Table 1. Due to the severity of nystagmoid eye

Table 1
Clinical and genetic characteristics of patients

ID	Age (years)/ sex	*PAX6* mutation/11p13 deletion and genomic coordinates	Eye	AAK stage	Superior limbus		Inferior limbus		LSCM parameters		
					LSCM	AS-OCT	LSCM	AS-OCT	Conjunctival islands	Goblet cells	"Cracked earth"-like images[a]
1A	26/f	heterozygous deletion: *DCDC1−ELP4ex9* hg18;;chr11:31 285 887−31 628 232	OD	0	full	full	full	full	-	–	+
			OS	0	full	full	full	full	–	–	+
1B	30/f	heterozygous deletion: *DCDC1−ELP4ex9* hg18;;chr11:31 285 887−31 628 232	OD	0	partial	–	full	full	–	–	+
			OS	0	partial	–	full	full	–	–	+
2	35/f	heterozygous deletion: *DCDC1−ELP4ex9* hg18;;chr11:31 285 887−31 628 232	OD	0	–	–	partial	partial	–	–	+
			OS	0	–	–	partial	partial	–	–	+
3	45/f	no mutation found	OD	0	partial	–	partial	partial	–	–	+
			OS	0	partial	–	partial	partial	–	–	+
4A	29/m	c.829C>T ex10	OD	1	partial	nst	partial	nst	+	–	+
			OS	2	–	nst	–	nst	+	+	–
4B	56/f	c.829C>T ex10	OD	2	–	–	–	–	+	+	–
5	49/m	c.−125dupG ex3	OD	1	–	–	–	–	+	+	–
			OS	1	–	–	–	–	+	+	–
6A	4/m	c.491delC ex7	OD	1	–	–	–	–	+	–	–
			OS	1	–	–	–	–	+	–	–
6B	27/f	c.491delC ex7	OD	2	–	–	–	–	+	–	–
			OD	2	–	–	–	–	+	–	–
7A	10/f	c.1183G>T ex12	OD	1	–	–	–	–	+	–	–
			OS	1	–	–	–	–	+	–	–
7B	35/f	c.1183G>T ex12	OD	3	–	–	–	–	vascularization	+, numerous cells	–
			OS	4	–	–	–	–	vascularization	+, numerous cells	–
8	14/f	c.1268A>T ex13	OD	1	–	–	–	–	+	+, single cells	–
			OS	1	–	–	–	–	+	+, single cells	–
9	12/f	heterozygous deletion: *DCDC1ex1−ELP4−PAX6int1* hg18;;chr11:31 347 785−31 794 631	OD	1	nst	nst	nst	nst	nst	nst	nst
			OS	1	nst	nst	nst	nst	nst	nst	nst
10A	17/m	c.794G>A ex10	OD	1	–	–	–	–	–	–	–
			OS	1	–	–	–	–	–	–	–
10B	25/m	c.794G>A ex10	OD	2	–	–	–	–	+	–	–
			OS	1	–	–	–	–	–	–	–
10C	51/f	c.794G>A ex10	OD	1	–	–	–	–	+	+	–
			OS	1	–	–	–	–	+	+	–
11	28/m	c.78delG ex5	OD	1	–	–	–	–	+	+	–
			OS	2	nst	nst	nst	nst	+	+	–
12	29/m	genetic testing not done	OD	1	–	–	–	–	–	–	–
			OS	1	–	–	–	–	–	–	–
13	33/m	c.1032+6T>G int11	OD	1	–	–	–	–	+	–	–
14	26/m	heterozygous deletion: *PAX6ex5−PAX6ex7* hg18;;chr11:31 778 912−31 780 904	OD	1	–	–	–	–	+	–	–
			OS	4	–	–	–	–	vascularization	+	–
15	43/m	c.114_117dup ex5	OD	1	–	–	–	–	+	+	–
			OS	1	–	–	–	–	+	+	–
16	25/f	c.718C>T ex9	OD	2	–	nst	–	nst	+	+	–
			OS	2	–	–	–	–	+	+	–
17	35/f	c.411delG	OD	2	–	–	–	–	+	–	–
			OS	2	–	–	–	–	+	–	–
18	30/f	c.142−5T>G int5	OD	3	–	–	–	–	vascularization	+	–
			OS	2	–	–	–	–	+	+	–
19A	37/m	heterozygous deletion: *PAX6ex3* hg18;;chr11:31 784 748−31 787 957	OD	2	–	–	full	full	+	–	nk
19B	53/m	heterozygous deletion: PAX6ex3 hg18;;chr11:31 784 748−31 787 957	OS	2	nst	nst	partial	–	+	–	+
20A	51/m	c.141+4A>G int5	OD	3	–	–	–	–	+	+, numerous cells	–
			OS	3	–	–	–	–	+	+, numerous cells	–

(*continued on next page*)

Table 1 (*continued*)

ID	Age (years)/ sex	*PAX6* mutation/11p13 deletion and genomic coordinates	Eye	AAK stage	Superior limbus		Inferior limbus		LSCM parameters		"Cracked earth"-like images[a]
					LSCM	AS-OCT	LSCM	AS-OCT	Conjunctival islands	Goblet cells	
20B	56/m	c.141+4A>G int5	OD	3	–	–	–	–	+	+, numerous cells	–
			OS	3	–	–	–	–	+	+, numerous cells	–
21	26/f	c.265C>T ex6	OD	2	–	–	–	–	+	+	–
			OS	3	–	–	–	–	vascularization	+	–
22	42/f	heterozygous deletion: *ELP4ex9–PAX6–RCN1– WT1ex1* hg18:;chr11:31 628 232–32 413 841	OD	3	–	–	–	–	vascularization	+	–
			OS	3	nst	nst	nst	nst	nst	nst	nst
23	27/m	c.766-2A C ex10	OD	3	–	–	–	–	vascularization	+	–
			OS	4	–	–	–	–	vascularization	+	–
24	49/m	no mutation found	OD	5					eyeball subatrophy		
			OS	3	–	–	–	–	vascularization	+	–

PAX6 coordinates: 31 762 916–31 789 477 (hg18)
PAX6 mRNA Transcript Variant (1) NM_000280.4
[a] the typical "cracked" appearance of the epithelium in the corneal limbus region: dark curvilinear columns or streaks, interrupting the regular mosaic of basal cells; AAK = aniridia-associated keratopathy; LSCM = laser scanning confocal microscopy: AS-OCT = anterior segment optical coherence tomography; m = male, f = female, "–" = not present; "+" = present; full = normal appearing palisades; partial = distorted palisades or palisade-like structures; nst = nystagmus prevented correct diagnostic procedure; vascularization = conjunctival/metaplastic cells on the center of the cornea with vessels present; nk = not known, indicates no image data was obtained.

movements and no gaze fixation, it was impossible to perform confocal microscopy in 5 eyes. For the same reasons, AS-OCT image analysis was impeded in 9 eyes.

In 4 patients (8 eyes), biomicroscopy revealed completely transparent cornea without signs of limbal insufficiency (stage 0 AAK). One of the siblings (1A) with a family history of aniridia and a chromosomal rearrangement 11p13 at the level of *DCDC1* и *ELP4* genes, a 3′ *cis*-regulatory region for *PAX6,* showed unaffected POVs in both superior and inferior limbus. Cataract extraction and artificial iris-lens diaphragm was performed on one eye of this patient with cornea transparent for 3 years of follow-up. The morphology of progenitor structures in both eyes was fully preserved and consistent with the confocal microscopy pattern in healthy individuals. Structure of limbal crypts in the superior hemisphere of the cornea had a reticulate pattern with POVs in the inferior half appearing in the form of classic pale fence; dark zone of curvilinear columns or streaks was well-visualized (showing alternation of hyper- and hyporeflective areas of basal epithelium) as described previously in healthy subjects [20,21]. In Cornea Cross Line protocol, the corneoscleral transition zone was observed with gradual change from optically clear corneal epithelium to more opaque conjunctival epithelium. En Face mode AS-OCT in limbal areas provided POV images of clear hyperreflective lines with well visualized details similar to LSCM images (Fig. 1).

In contrast, images from the second sibling (1B) with the same mutation manifested significantly altered POV structure in the superior limbus. Limbal crypts were poorly differentiated with thickened hyper-reflective palisade-like lumps with indistinct contours and solitary FSPs. AS-OCT was of little assistance in visualizing limbal structures reliably. Short palisade ridge remnants were not visible; instead a hyporeflective strip at the level of basal epithelium was detected. At the same time, a study of the inferior limbus showed intact POVs as hyper-reflective linear fence-like structures – a finding confirmed by LSCM (Fig. 2).

A 35-year-old patient (2) with no clinical signs of AAK and the same deletion of 11p13 3′ *cis*-regulatory region for *PAX6* presented disturbed palisades on LSCM in the inferior circumference. Her AS-OCT tomograms in the inferior limbus revealed less evident shortened crypts, which lost palisade appearance and prominent contours, though still discernible and recognizable.

In patient 3, who was 45 years of age and with confirmed absence of *PAX6* gene mutation, localized areas of altered limbal structure in superior and inferior limbus circumferences were found. Despite a history of intraocular surgery (cataract extraction with implantation of iris-lens diaphragm on both eyes), no progression of AAK was evident in this patient, with cornea remaining intact throughout the 4-year follow-up period. En Face AS-OCT showed limbal crypts in the inferior limbus only; in the superior half distorted POVs were not reliably detected (Fig. 3).

Nystagmus was absent in all patients with stage 0 AAK, which allowed good visualization of limbal zone structures by LSCM and avoided additional noise and ghosting in AS-OCT images. In all cases, corneal-type epithelium with no signs of conjunctival invasion was resolved in the limbal zone as well as an area of curvilinear "tracks" in the form of hyper- and hyporeflective regions of basal epithelium stemming from POV apices and extending toward the corneal center. POVs were best imaged by En Face AS-OCT, when scan depth was aimed at Bowman's membrane or somewhat lower.

Stage I AAK as manifested by typical peripheral corneal opacity was diagnosed in 13 patients (21 eyes). In the eye of one patient (4A) with stage I AAK, palisade-like structures that significantly differed from normal limbal crypts were found on the background of mild clinical signs. POV visualization using AS-OCT in En Face

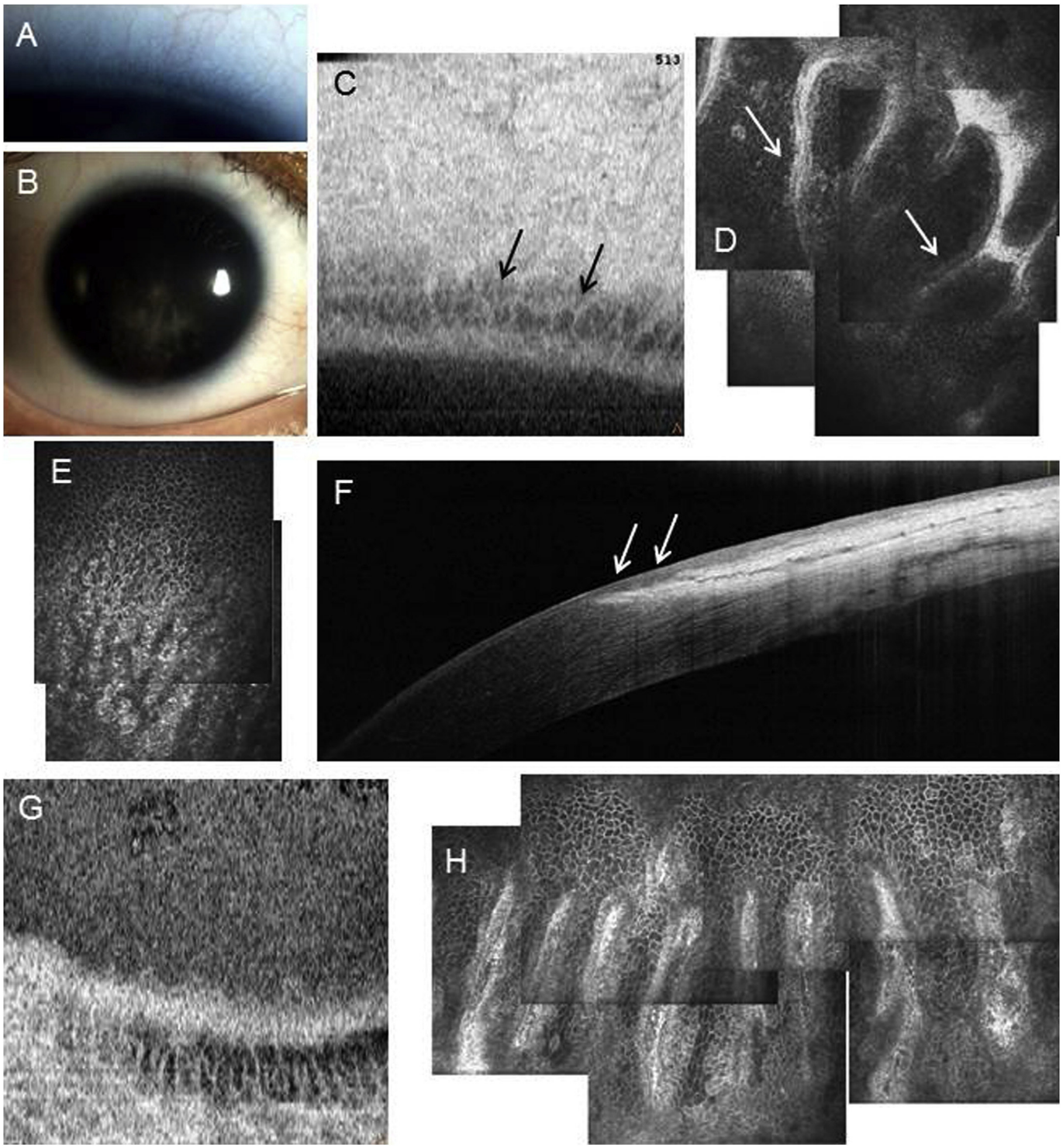

Fig. 1. Examination data of the right eye of patient 1A, 26 years old, stage 0 AAK. (A, B) Slit lamp image indicates a transparent cornea, cortical lens opacities, and no visible iris. (C) AS-OCT image of the superior limbus in En Face mode: a mesh structure of POV is seen (arrows). (D) LSCM image of the same section as in C, POVs, surrounded by bright halo of limbal basal cells, are indicated by arrows. (E) Typical appearance of the zone of "streams," "cracked earth": alternating hyper- and hypo-reflective areas of the basal epithelium. (F) AS- OCT image of the superior limbus obtained using Cornea Cross Line protocol: corneoscleral transition zone with a gradual change of optically transparent corneal epithelium to more optically dense conjunctival epithelium is visible; arrows indicate limbal epithelium location. (G) AS- OCT image of the inferior limbus in En Face mode: hyper-reflective parallel lines are seen. (H) LSCM image of an identical area of the inferior limbus: intact POVs are visible, basal limbal epithelium is well visualized in the inter-palisade space.

mode in this patient was hampered by pronounced nystagmus.

In other stage I AAK eyes, limbal progenitor structures were not identified. On the corneal periphery, one could observe conjunctival tissue invasion in the form of conjunctival outgrowths or islands of varying extent. Destruction of limbal barrier was accompanied by the appearance of single inflammatory and goblet cells in the cornea (Fig. 4A). While mosaic structure of basal cells had been preserved and cells maintained normal corneal

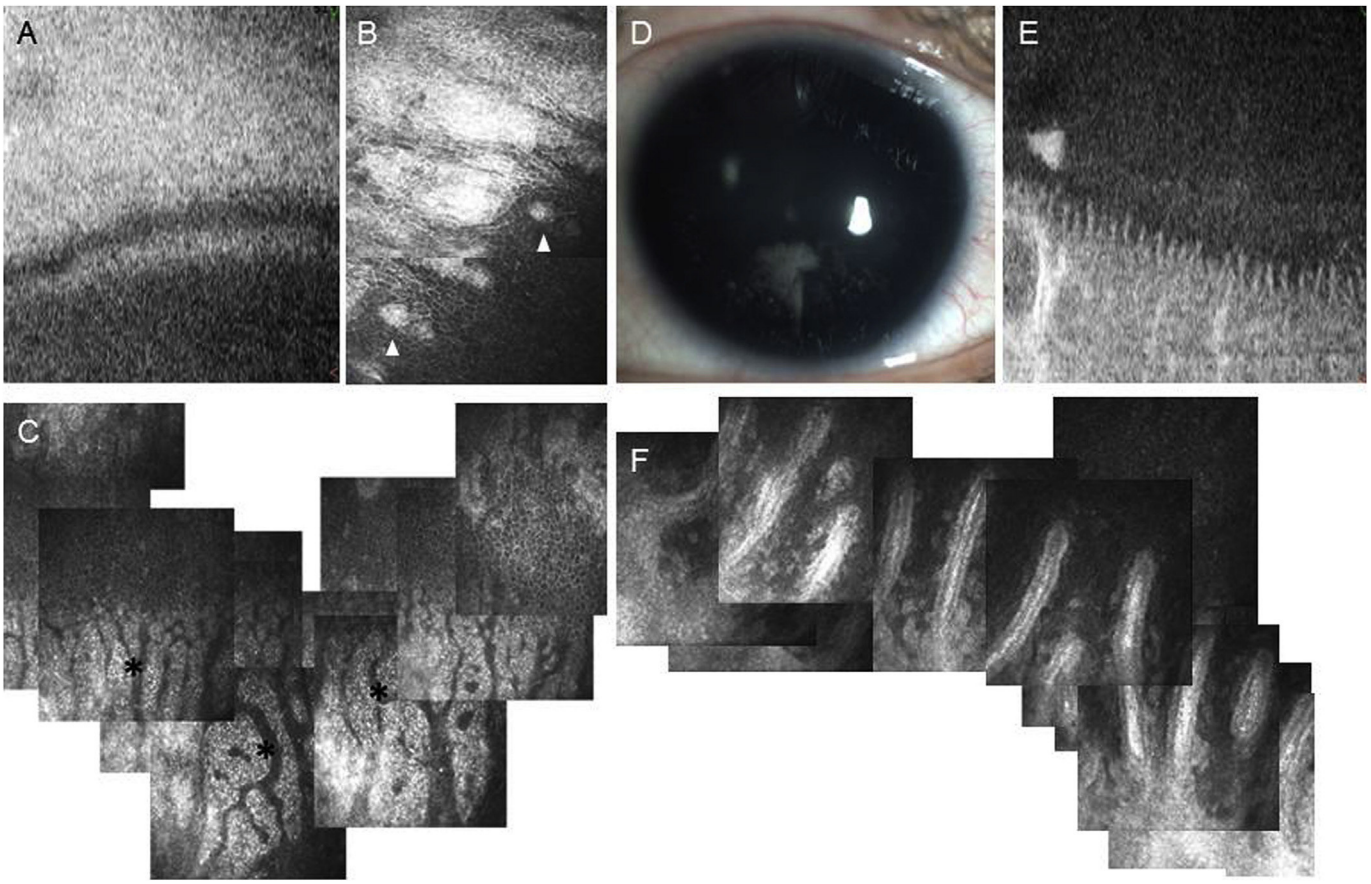

Fig. 2. Examination data of patient 1B, 30 years old, stage 0 AAK. (A–C) Examination of the superior limbus. (A) POVs are not visualized in the OCT images. (B) LSCM images show shortened hyper-reflective palisade-like structures (arrows), FSPs are marked by triangular arrows. (C) Wide zone of "streams" (asterisks) interrupting the mosaic pattern of the basal epithelium and propagating toward the center of the cornea is visible. (D) Slit lamp image indicating a transparent cornea without signs of keratopathy, partial opacity of the lens and no visible iris. (E) AS-OCT images show conspicuous POVs in the inferior half of the cornea in the form of a pale fence arranged in parallel. (F) LSCM images of the same area as in (E) show similar structure of POVs that correlates with SD-OCT images in En Face mode.

phenotype, cell boundaries were less distinct. In 4 cases, prominent cell nuclei could be visualized in wing and basal cell layers (Fig. 4B). Neither AS-OCT nor LSCM could pinpoint limbal progenitor structures in a 4-, 10- and 12-year-old patients with stage I AAK. In En Face mode, in the area of supposed POV localization, a uniform monochromatic hyper-reflective band with no internal structure to it was identified (Fig. 5).

Out of 10 patients (13 eyes) with stage II AAK, two related patients (19A, 19B [2 eyes]) with a deletion of one *PAX6* gene exon (*PAX6ex3* del) showed altered, partially deformed POV structure in the inferior half of the limbus (Fig. 4C). In other eyes, progenitor structures were not identified, while emerging signs of epithelial conjunctivalization with invasion of numerous inflammatory and goblet cells was clearly evident. Metaplastic corneal epithelium exhibiting conjunctival phenotype of light nuclei and indistinct contours reached corneal mid-periphery and center in 9 eyes (Fig. 4D).

In 10 stage III and 3 stage IV eyes, epithelial damage extended to corneal center with predominance of neovascularization and subepithelial stromal opacification. All sub-populations of epithelial cells and keratocytes were affected, with complete destruction of optical surface. Goblet cells formed crypt-like clusters and were present in large numbers along the newly formed blood vessels (Fig. 4E-I). "Cracked earth"- like images were not detected in stage III-IV patients. AS-OCT images were in line with those of LSCM manifesting no POVs (Fig. 6).

Correlation analysis of cross-mode diagnostic consistency for POV visualization in the inferior limbus between LSCM and AS-OCT revealed strong positive correlation ($r_S = 0.85$, $P < 0.05$). The Spearman's rank correlation coefficient for the superior limbus was slightly lower ($r_S = 0.53$, $P < 0.05$). Whenever intact POVs were detected on LSCM, characteristic appearance of progenitor structures was well visualized on AS-OCT panoramic images. The inconsistency in the results of the two diagnostic methods was observed, if limbal crypts were deformed, smaller in size or seen in a small proportion of LSCM frames. Of 11 cases with palisade-like structures or partially present POVs on LSCM, similar structures were identified by AS-OCT in 4 eyes, in 5 eyes limbal crypts were not reliably detected, and in 2 eyes evaluation was prevented by severe nystagmus.

The negative relationship between clinical AAK stage and preservation of progenitor limbal structures on in vivo imaging ($r_S = -0.5$, $P < 0.05$) was demonstrated, while the association between AAK stage and patient age ($r_S = 0.235$, $P = 0.209$) did not reach statistical significance.

4. Discussion

Along with glaucoma and cataract, AAK is the leading cause of progressive visual loss in patients with congenital aniridia. Loss of transparency in central cornea due to centripetal growth of vascularized pannus or formation of white and gray Salzmann nodules

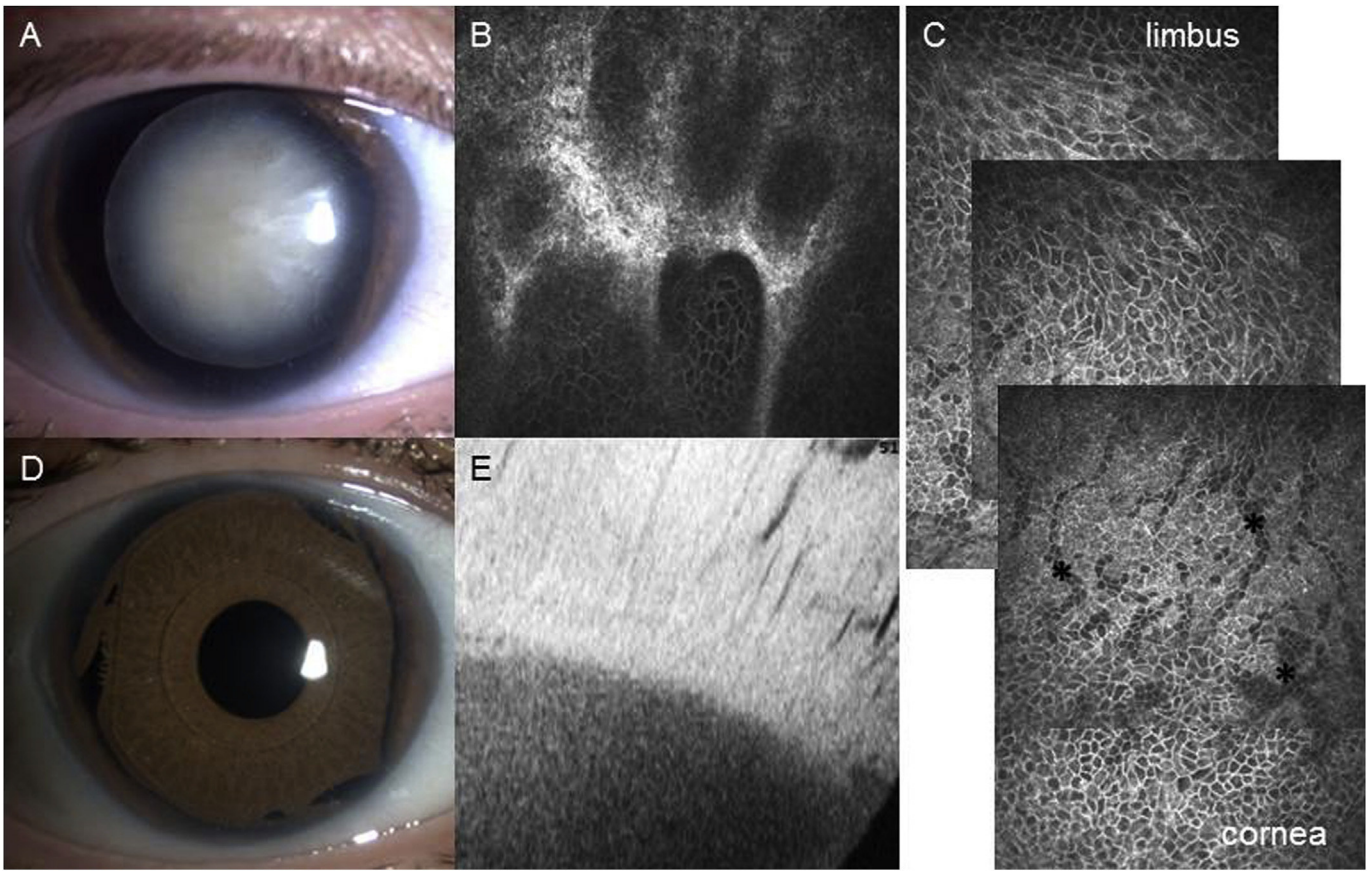

Fig. 3. Images of the superior limbus of patient 3, aged 45 years with stage 0 AAK. (A) Preoperative slit lamp image: partial aniridia, total cataract, no keratopathy. (B) LSCM images show shortened limbal crypts; basal epithelium pattern is intact. (C) Multiple-crop LSCM image depicts typical "cracked" appearance of the epithelium in the superior half of the limbus (asterisks). (D) Slit lamp image 4 years post-surgery: partial aniridia, iris-lens diaphragm, corneal transparency is preserved. (E) POVs are not visualized in the AS-OCT images.

in the optical center is usually observed at the age of 18–20 years. Optically significant corneal opacity progresses over time, causing blindness in aniridic patients older than 30 years in 37% of cases. The natural progression of AAK can be aggravated by surgical procedures that damage limbal stem area. However, in spite of the growing prevalence of AAK with age [14,22], several cases were reported with no corneal changes in patients with aniridia in older age groups [19,23,24]. In our study as well, LSCM in three adult patients (1A, 1B, 2) reliably showed the presence of POVs in the limbal zone and intact corneal-type epithelial cells (Figs. 1 and 2). The genetic defect in these cases affecting 3′ *cis*-regulatory regions abrogates *PAX6* gene expression [25,26] and resulted in the development of aniridia phenotype. The first morphological demonstration of limbal progenitor structures in patients with this mutation in our study may explain the lack of AAK and transparency of the corneal surface in older patients and after surgical interventions. The presence of a mechanism that makes it possible to preserve functioning LSCs in *PAX6* haploinsufficiency requires further study and analysis.

Partial preservation of limbal stem structures without clinical signs of LSCD was discovered in one more patient with aniridia (patient 3). A similar case of stage 0 AAK with intact POVs on confocal microscopy was described in a 54-year-old patient with a history of intraocular surgery [19]. In these two clinical cases, *PAX6* gene mutation was not verified.

Therefore, clinical diagnosis of congenital aniridia does not exclude the presence of limbal structures with intact progenitor function maintaining regeneration and self-renewal of the corneal epithelium, as well as sustaining long-term ocular surface transparency even after surgical procedures.

Altered degraded limbal palisades were also found in the inferior half of the cornea at stages I (one eye) and II (2 eyes) of AAK. POVs were visualized in only one eye in the superior limbus. In a study of correlation between AAK stage and LSCD severity [19], palisade-like structures were observed in the inferior limbus only in stage I AAK (5 eyes). The authors attributed the absence of limbal crypts in stage II eyes to the progression of limbal insufficiency. We have also identified a negative correlation between preservation of progenitor limbal structures and AAK stage, although somewhat weaker ($r_S = -0.5$, $P < 0.05$).

One of the specific findings on LSCM of limbus is regions of non-uniform reflectivity of the basal epithelium central to the POVs. These regions of so-called "cracked earth" or curvilinear "tracks" are visualized in healthy individuals without LSCD signs [20,21]. According to Townsend et al., such a mosaic pattern where hyper- and hypo-reflective areas, "streams," alternate is associated with centripetal movement of basal epithelial cells to replace the pool of cells in central cornea [27]. In aniridia, due to mutations in the *PAX6* gene, epithelial cell capacity to migrate is compromised, which is one of the underlying causes of AAK progression [28]. LSCM imaging in patients with aniridia revealed the presence of typical "cracked earth" pattern in all eyes with detected limbal progenitor structures (Table 1, Figs. 1–3). In our view, the identification of such a transit zone in patients with suspected LSCD is a good prognostic

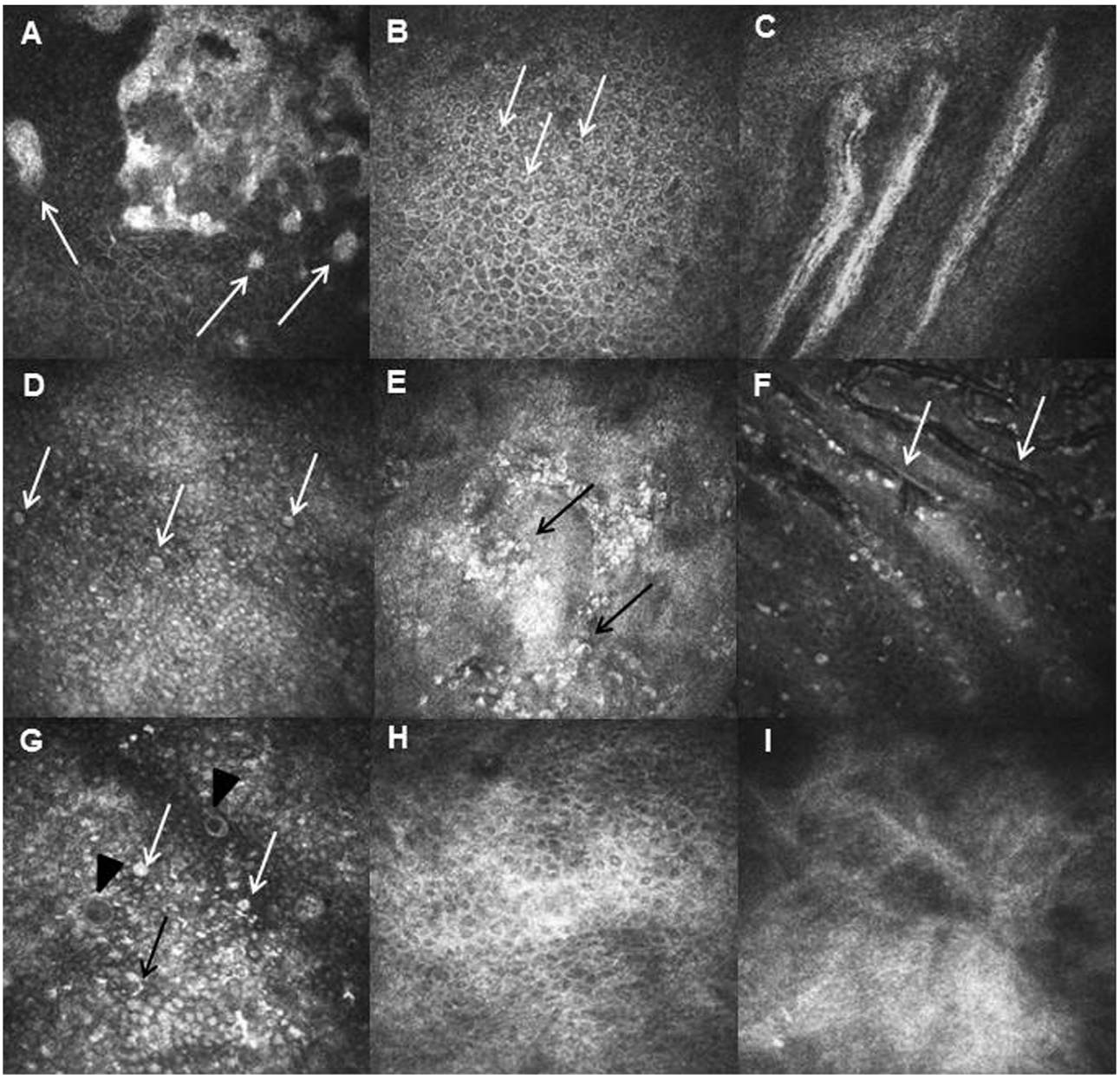

Fig. 4. LSCM images of morphological changes in the limbal zone at different grades of AAK. (A,B) Stage I AAK. (A) Transition zone between corneal and conjunctival epithelium: initial invasion of conjunctival tissue in the form of islands are seen (arrows). (B) Image shows wing and basal epithelial cells with bright activated nuclei (indicated by arrows) and indistinct contours. (C,D) Stage II AAK. (C) Altered limbal POVs arranged in the form of parallel lines; due to severe nystagmus, cells are not clearly visualized in the inter-palisade space. (D) Conjunctival metaplasia of corneal epithelium: cells exhibit larger hyper-reflective nuclei, cell borders are not defined, multiple goblet (arrows) cells are seen. (E–I) Stage III-IV AAK. (E) Goblet cells crypt (arrows); epithelial cell structure is not visible. (F) Corneal neovascularization: clearly visible blood vessels at the level of wing-like epithelium (arrows). (G) Conjuctivalization of corneal epithelium: disordered cell arrangement, loss of cell borders, enlarged activated cell nuclei, intraepithelial cystic changes (black arrowheads), multiple inflammatory (black arrow indicates a leukocyte) and goblet cells (indicated by white arrows). (H) Conjuctivalization of the cornea: visualized cells are phenotypically similar to the basal conjunctival epithelium. (I) Loss of cellular structure in corneal epithelium, complete destruction of corneal surface, cicatricial changes cover the entire epithelial layer. All images 400 × 400 μm.

indicator pointing to the intact germinal function of LCSs even in cases of difficult visualization of POVs and FSPs in patients with nystagmus, impaired sight fixation just like in the case of aniridia.

Time of onset and appearance of early signs of AAK are variable, usually corresponding to 10 years of age according to the literature [5]. The youngest age at which signs of peripheral corneal opacity were found is 14 months [29]. In our study, LSCM and AS-OCT of the limbal area in children and adolescents with aniridia aged 4 (6A), 10 (7A) and 12 (8) were performed for the first time. Clinically, stage I AAK was diagnosed in these young patients, but in all of them limbal palisades were not detectable. Morphologically, in some children an invasion of conjunctival tissue in the cornea was detected as small islets with single goblet cells (Fig. 5). Their parents aged 27 (6B) and 35 (7B), who had no history of ocular surgery, manifested AAK progression to stages II and IV, respectively.

However, in children, despite absent progenitor structures and impaired limbal barrier, corneal epithelium remains compensated for a long time. The reason for this stability is not completely clear nor is it consistent with the development rate of corneal changes in LSCD due to other causes (chemical burns, Stevens-Johnson

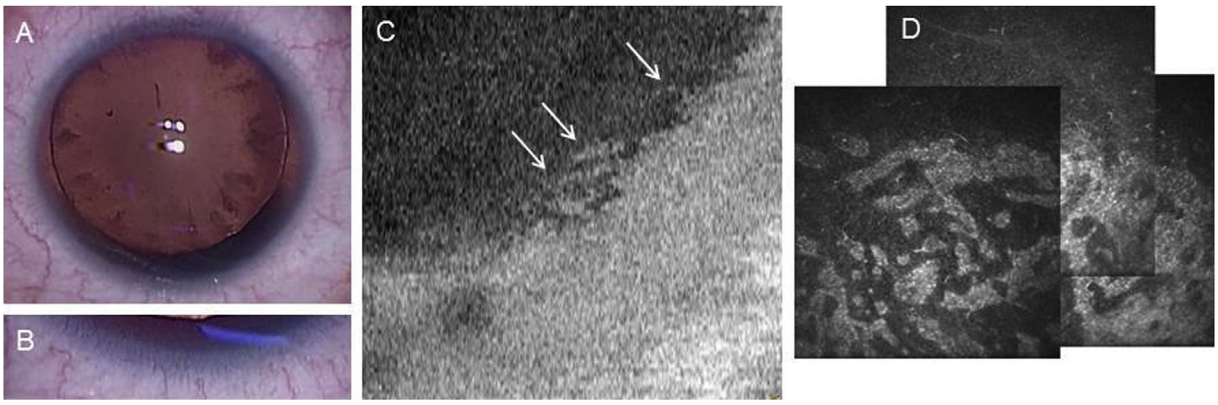

Fig. 5. Examination data of patient 7A, aged 10, with stage I AAK. (A, B) Slit lamp image: superficial mild peripheral corneal opacity, total aniridia, partial cataract. (C) AS-OCT fails to depict POVs in the inferior limbus, clearly visible conjunctival islets (arrows). (D) LSCM images also show multiple conjunctival islands.

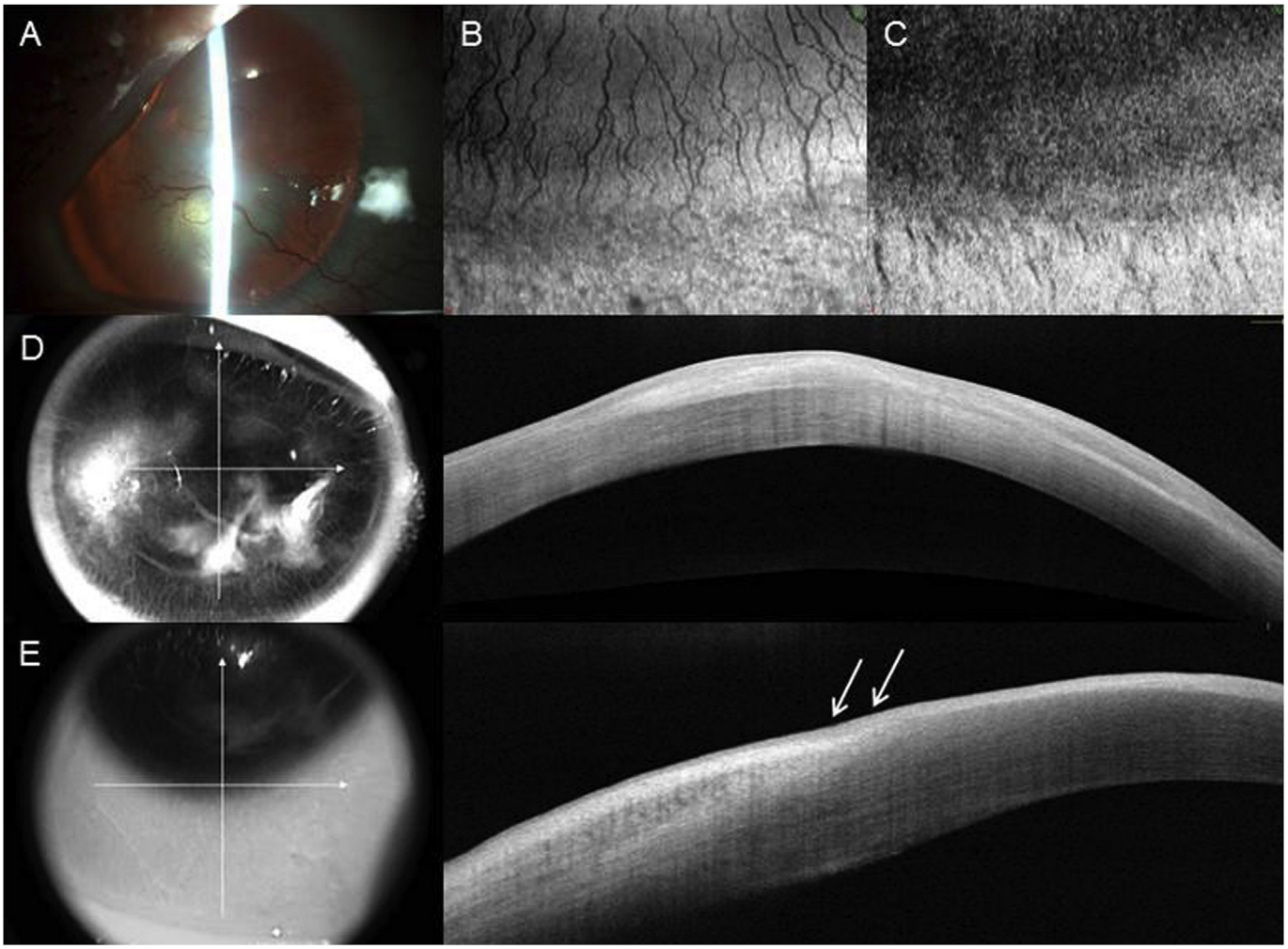

Fig. 6. Examination data of patient 7B, aged 35, with stage IV AAK. (A) Slit lamp image: central and peripheral subepithelial corneal opacities with neovascularization. (B) AS-OCT image in 3D Cornea protocol (SLO mode): clearly visible superficial newly formed blood vessels of the inferior half of the cornea. (C) AS-OCT image in 3D Cornea protocol (En Face mode): POVs are not visualized. (D) AS-OCT image of the central cornea obtained via Cornea Cross Line protocol: subepithelial scar is clearly visible in the form of hyper-reflective structure propagating to the central stromal layers, corneal thickness in the scarred area is increased significantly. (E) AS-OCT image of the inferior half of the limbus obtained via Cornea Cross Line protocol: vertical section shows a homogeneous coloring of the conjunctival and corneal epithelium, no difference in the optical density of the epithelial layer, the transition zone is smoothed (arrows).

syndrome, ocular cicatricial pemphigoid). In other types of total LSCD, the optical zone of the cornea opacifies within a short time period ranging from several weeks to months. The mechanism that prevents the spread of circular peripheral opacity to central cornea

in AAK and keeps the optical center transparent for several years is currently not fully understood. Apparently, the same unknown mechanism preserves the central corneal zone in adult patients. Ihnatko et al. hypothesized that slow phased progression of keratopathy could be explained by LSC availability and functional limbal barrier in early AAK. Remaining LSCs give rise to cells of both corneal and conjunctival phenotype migrating to the center of the cornea. With keratopathy progression, gradual POV degradation leads to cessation of corneal epithelial cell replenishment, disruption of limbal barrier, and prompt conjunctival pannus overgrowth [30].

Nubile et al. reported complete absence of POVs in 50% of patients with clinical signs of partial LSCD. Despite undetectable limbal progenitor structures in these patients, maintenance of corneal-type epithelium in central and paracentral cornea was observed [13]. Furthermore, recent studies have demonstrated the long-term survival of normal corneal epithelial islets in central cornea in limbal deficiency spanning 360° [31]. The authors suggest that a small number of LSCs, which, despite destruction of their "niches," are able to survive and give rise to corneal-phenotype epithelial cells, or that the basal transient amplifying cells of the central surviving epithelium are independently capable of maintaining the overlying cell mass for a long period of time. In our study we observed two patients aged 43 (15) and 51 (10C) with no identifiable limbal progenitor structures on confocal microscopy and clinically defined stage I AAK.

Thus, notwithstanding the association of keratopathy progression and patient age noted in some earlier reports, in our study as well as in that of Lagali et al. [19], the above-mentioned correlation was found to be statistically insignificant. In the majority of aniridic patients, including children, in a *PAX6*-deficient state, limbal progenitor structures are not detectable that could be a reason for AAK development and progression. The rate of AAK progression in different patients with seemingly equal starting conditions (genetic cause, ocular surgery absence, non-detectable POVs on in vivo imaging) is variable. Given that apparent multi-level heterogeneity in the study cohort (demographic and genetic characteristics) it is difficult to expect straightforward correlation of AAK severity and patient age in our study. Also, a considerable proportion of patients with 3′ mutations and intact POVs in our study group made it harder to establish this correlation.

To the best of our knowledge, this study represents the first attempt to assess the diagnostic value and correlation of in vivo limbal palisade imaging by LSCM and En Face AS-OCT in aniridic patients. LSCM is the most important diagnostic tool that allows clinicians to study in vivo cellular morphology of the ocular surface – all layers of the cornea, conjunctiva, and limbus. LSCM is a mandatory test in the workup of patient with LSCD [32–35]. However, aniridic patients are not always good candidates for LSCM due to its known limitations. It requires corneal contact necessitating use of local anesthetics. Pronounced ptosis and nystagmus pose serious challenges for obtaining valuable images in any patient, and considerable duration and complexity of the method limits its applicability to a younger patient population.

Currently, the diagnostic capabilities offered by OCT are not just limited to evaluation of vitreoretinal pathology. AS-OCT run in different modes allows visualization of POVs, limbal vascular arcades, sub-basal nerve plexuses [36], measurement of corneal and limbal epithelial thickness [37,38], and act can serve as an alternative diagnostic method [39,40]. Previous reports show a high degree of correlation between the images of POVs provided by AS-OCT and LSCM in healthy subjects [40] and on cadaver eyes [39,41]. Contrary to single-field scans on LSCM, panoramic AS-OCT images of the lower and upper limbus provide information on the extent, shapes, and patterns of limbal crypts and FSPs. The extensive outlook and acquisition speed of the images, low retest variability, and registration of clinical data make AS-OCT an attractive diagnostic tool for dynamic studies of limbal anatomy. High fidelity of the tomograms allows side-by-side comparisons of identical locations on LSCM and AS-OCT and follow-up of regions of interest. Because of the high correlation of LSCM and AS-OCT images in healthy subjects ($r_S = 0.99$, $P < 0.05$) [40], we applied these imaging modalities to evaluation of patients with limbal insufficiency. Our extrapolation of this methodology to aniridic patients revealed a high level of correlation ($r_S = 0.85$, $P < 0.05$) for the inferior limbus with a less powerful correlation for the superior cornea ($r_S = 0.53$, $P < 0.05$). In every eye where intact POVs were observed by LSCM, a characteristic pattern of limbal progenitor structures was well visualized on panoramic AS-OCT imaging. However, the sensitivity of the latter diminished when dealing with altered, trimmed POVs, preferentially located in the superior limbus. In healthy subjects, superior limbal structures are more variable in shape, usually thinner, and often reveal a mesh-like pattern. POV spacing in the superior corneal hemisphere is less regular as opposed to well-delineated radially oriented palisades of the inferior limbus [11,21,27,39,40,42]. In early AAK (stage 0-I), palisades in the superior half of the cornea often appear as truncated deformed palisade-like lumps, and they are difficult to visualize with LSCM. AS-OCT performed in 3D Cornea protocol (En Face mode) in these patients does not provide unequivocal POV images, accounting for lower consistency between two diagnostic methods for the superior limbus. In the four instances, when partially present POVs of superior limbus were detected on LSCM, their contours on AS-OCT were either not clearly visible, or hardly distinguishable from overlying blood vessel shadows or deeper lying scleral fibers at the corneoscleral junction. Contrary to superior limbus, partially distorted though wider and more hyper-reflective crypts of the lower limbus are better visualized by both techniques (Table 1). In our opinion, diminution of diagnostic value of AS-OCT in detection of altered distorted upper hemisphere POVs may be explained by regional peculiarities in limbal tissue architecture. However, this assumption requires validation from further analysis in a wider cohort of patients. In the absence of limbal progenitor structures, AS-OCT was useful in the longitudinal evaluation of the extent of conjunctival outgrowths.

Advantages of AS-OCT in limbal examination include its non-contact nature, high scanning resolution, speed and area, easy patient tolerability and applicability to a pediatric population. Nonetheless, given the limited number of cases with detected POV in our cohort, it is impossible to assess reliably the sensitivity of AS-OCT in detecting deformed POV with relation to their location (superior or inferior limbus) and degree of damage. Further studies of diagnostic utility of En Face AS-OCT are warranted in larger patient populations including alternative causes of LSCD. The most important limiting factor for the application of AS-OCT in aniridic patients was nystagmus, the magnitude and speed of which in some cases preclude obtaining high-quality images. In our study, considerable nystagmoid eye movements hampered AS-OCT procedure in 15% of cases, while for LSCM it was in 8.2% of the eyes.

5. Conclusion

Modern diagnostic equipment has enabled clinicians to visualize progenitor limbal structures in unprecedented detail and evaluate LSCD severity. Confocal microscopy remains the "gold standard" for imaging of corneal morphological changes in vivo. LSCD progression in AAK manifests itself with limbal barrier disruption, propagation of conjunctival epithelium to the central areas of the cornea and emerging goblet and inflammatory cells on its surface, degradation or complete destruction of POVs. LSCM

allows visualization of changes that occur at different stages of AAK as well as evaluation of corneal epithelium health. There is a negative correlation between AAK stage and the morphological integrity of progenitor limbal structures.

AS-OCT as performed in En Face mode of 3D Cornea protocol represents an alternative imaging tool for limbal palisades examination in patients with compromised limbal function.

In spite of clinical observations of gradual AAK progression with age and following surgical interventions damaging the limbal zone, aniridic patients exhibit different rates of corneal epithelial decompensation. Further research into genetically mediated aspects of AAK is necessary as well as search for alternative ways to maintain epithelial integrity.

Conflicts of interest

The authors have no commercial or proprietary interest in any concept or product described in this article.

References

[1] Hingorani M, Hanson I, van Heyningen V. Aniridia Eur J Hum Genet 2012;20:1011–7. http://dx.doi.org/10.1038/ejhg.2012.100.

[2] Robinson D, Howarth R, Williamson K, van Heyningen V, Beal S, Crolla J. Genetic analysis of chromosome 11p13 and the PAX6 gene in a series of 125 cases referred with aniridia. Am J Med Genet A 2008;146A:558–69. http://dx.doi.org/10.1002/ajmg.a.32209.

[3] Nelson LB, Spaeth GL, Nowinski TS, Margo CE, Jackson L. Aniridia. A review. Surv Ophthalmol 1984;28:621–42.

[4] Grønskov K, Olsen JH, Sand A, Pedersen W, Carlsen N, Bak Jylling AM, et al. Population-based risk estimates of Wilms tumor in sporadic aniridia. A comprehensive mutation screening procedure of PAX6 identifies 80% of mutations in aniridia. Hum Genet 2001;109:11–8.

[5] Lopez-Garcia J, Garcia-Lozano I, Rivas L, Martinez-Garchitorena J. Congenital aniridia keratopathy treatment. Arch Soc Esp Oftalmol 2006;81:435–44.

[6] Nishida K, Kinoshita S, Ohashi Y, Kuwayama Y, Yamamoto S. Ocular surface abnormalities in aniridia. Am J Ophthalmol 1995;120:368–75.

[7] Ramaesh T, Collinson JM, Ramaesh K, Kaufman MH, West JD, Dhillon B. Corneal abnormalities in Pax6+/- small eye mice mimic human aniridia-related keratopathy. Invest Ophthalmol Vis Sci 2003;44:1871–8.

[8] Mohan R, Chintala SK, Jung JC, Villar WV, McCabe F, Russo LA, et al. Matrix metalloproteinase gelatinase B (MMP-9) coordinates and effects epithelial regeneration. J Biol Chem 2002;277:2065–72. http://dx.doi.org/10.1074/jbc.M107611200.

[9] Ramaesh K, Ramaesh T, Dutton G, Dhillon B. Evolving concepts on the pathogenic mechanisms of aniridia related keratopathy. Int J Biochem Cell Biol 2005;37:547–57. http://dx.doi.org/10.1016/j.biocel.2004.09.002.

[10] Chen Z, de Paiva CS, Luo L, Kretzer FL, Pflugfelder SC, Li DQ. Characterization of putative stem cell phenotype in human limbal epithelia. Stem Cells 2004;22:355–66. http://dx.doi.org/10.1634/stemcells.22-3-355.

[11] Shortt A, Secker G, Munro P, Khaw P, Tuft S, Daniels J. Characterization of the limbal epithelial stem cell niche: novel imaging techniques permit in vivo observation and targeted biopsy of limbal epithelial stem cells. Stem Cells 2007;25:1402–9. http://dx.doi.org/10.1634/stemcells.2006-0580.

[12] Kinoshita S, Adachi W, Sotozono C, Nishida K, Yokoi N, Quantock AJ, et al. Characteristics of the human ocular surface epithelium. Prog Retin Eye Res 2001;20:639–73.

[13] Nubile M, Lanzini M, Miri A, Pocobelli A, Calienno R, Curcio C, et al. In vivo confocal microscopy in diagnosis of limbal stem cell deficiency. Am J Ophthalmol 2013;155:220–32. http://dx.doi.org/10.1016/j.ajo.2012.08.017.

[14] Edén U, Riise R, Tornqvist K. Corneal involvement in aniridia. Cornea 2010;29:1096–102. http://dx.doi.org/10.1097/ICO.0b013e3181d20493.

[15] Takahashi N, Chikama T, Yanai R, Nishida T. Structures of the corneal limbus detected by laser-scanning confocal biomicroscopy as related to the palisades of Vogt detected by slit-lamp microscopy. Jpn J Ophthalmol 2009;53:199–203. http://dx.doi.org/10.1007/s10384-008-0661-4.

[16] Grieve K, Ghoubay D, Georgeon C, Thouvenin O, Bouheraoua N, Paques M, et al. Three-dimensional structure of the mammalian limbal stem cell niche. Exp Eye Res 2015;140:75–84. http://dx.doi.org/10.1016/j.exer.2015.08.003.

[17] Zheng T, Xu J. Age-related changes of human limbus on in vivo confocal microscopy. Cornea 2008;27:782–6. http://dx.doi.org/10.1097/ICO.0b013e31816f5ec3.

[18] Wiley L, SundarRaj N, Sun TT, Thoft RA. Regional heterogeneity in human corneal and limbal epithelia: an immunohistochemical evaluation. Invest Ophthalmol Vis Sci 1991;32:594–602.

[19] Lagali N, Edén U, Utheim TP, Chen X, Riise R, Dellby A, et al. In vivo morphology of the limbal palisades of Vogt correlates with progressive stem cell deficiency in aniridic-related keratopathy. Invest Ophthalmol Vis Sci 2013;54:5333–42. http://dx.doi.org/10.1167/iovs.13-11780.

[20] Miri A, Al-Aqaba M, Otri AM, Fares U, Said DG, Faraj LA, et al. In vivo confocal microscopic features of normal limbus. Br J Ophthalmol 2012;96:530–6. http://dx.doi.org/10.1136/bjophthalmol-2011-300550.

[21] Patel D, Sherwin T, McGhee C. Laser scanning in vivo confocal microscopy of the normal human corneoscleral limbus. Invest Ophthalmol Vis Sci 2006;47:2823–7. http://dx.doi.org/10.1167/iovs.05-1492.

[22] Macedo K, de la Paz MF, Toledo JA, Tressera F, Perez-Santonja JJ, Llopis-de Benito L, et al. Characteristics of the cornea and the ocular surface in a population of patients with congenital aniridia. J Emmetropia 2012;3:130–9.

[23] Wawrocka A, Budny B, Debicki S, Jamsheer A, Sowinska A, Krawczynski MR. PAX6 3' deletion in a family with aniridia. Ophthalmic Genet 2012;33:44–8. http://dx.doi.org/10.3109/13816810.2011.615076.

[24] Zhang X, Zhang Q, Tong Y, Dai H, Zhao X, Bai F, et al. Large novel deletions detected in Chinese families with aniridia: correlation between genotype and phenotype. Mol Vis 2011;17:548–57.

[25] Lauderdale JD, Wilensky JS, Oliver ER, Walton DS, Glaser T. 3' deletions cause aniridia by preventing PAX6 gene expression. Proc Natl Acad Sci U. S. A 2000;97:13755–9. www.pnas.org/cgi/doi/10.1073/pnas.240398797.

[26] Crolla JA, van Heyningen V. Frequent chromosome aberrations revealed by molecular cytogenetic studies in patients with aniridia. Am J Hum Genet 2002;71:1138–49. http://dx.doi.org/10.1086/344396.

[27] Townsend WM. The limbal palisades of Vogt. Trans Am Ophthalmol Soc 1991;89:721–56.

[28] Collinson JM, Chanas SA, Hill RE, West JD. Corneal development, limbal stem cell function and corneal epithelial cell migration in the Pax6+/- mouse. Invest Ophthalmol Vis Sci 2004;45:1101–8.

[29] Voskresenskaya A, Pozdeyeva N, Vasilyeva T, Khlebnikova O, Zinchenko R. Clinical features of congenital aniridia in children and teenagers. Russ Pediatr Ophthalmol 2016;3:121–9. http://dx.doi.org/10.18821/1993-1859-2016-11-3-121-129.

[30] Ihnatko R, Eden U, Fagerholm P, Lagali N. Congenital aniridia and the ocular surface. Ocul Surf 2016;14:196–206. http://dx.doi.org/10.1016/j.jtos.2015.10.003.

[31] Dua HS, Miri A, Alomar T, Yeung AM, Said DG. The role of limbal stem cells in corneal epithelial maintenance. Testing the dogma. Ophthalmology 2009;116:856–63. http://dx.doi.org/10.1016/j.ophtha.2008.12.017.

[32] Miri A, Alomar T, Nubile M, Al-aqaba M, Lanzini M, Fares U, et al. In vivo confocal microscopic findings in patients with limbal stem cell deficiency. Br J Ophthalmol 2012;96:523–9. http://dx.doi.org/10.1136/bjophthalmol-2011-300551.

[33] Le Q, Deng SX, Xu J. In vivo confocal microscopy of congenital aniridia-associated keratopathy. Eye 2013;27:763–6. http://dx.doi.org/10.1038/eye.2013.50.

[34] Deng SX, Sejpal KD, Tang Q, Aldave AJ, Lee OL, Yu F. Characterization of limbal stem cell deficiency by in vivo laser scanning confocal microscopy. Arch Ophthalmol 2012;130:440–5. http://dx.doi.org/10.1001/archophthalmol.2011.378.

[35] Chan EH, Chen L, Yu F, Deng SX. Epithelial thinning in limbal stem cell deficiency. Am J Ophthalmol 2015;160:669–77. http://dx.doi.org/10.1016/j.ajo.2015.06.029.

[36] Espana EM. En face optical coherence tomography imaging of corneal limbal stem cell niche. In: Lumbroso B, Huang D, Romano A, Rispoli M, Coscas G, editors. Clinical En Face OCT Atlas. Jaypee Brothers Medical Publishers; 2013. p. 78–9.

[37] Le Q, Chen Y, Yang Y, Xu J. Measurement of corneal and limbal epithelial thickness by anterior segment optical coherence tomography and in vivo confocal microscopy. BMC Ophthalmol 2016;16:163. http://dx.doi.org/10.1186/s12886-016-0342-x.

[38] Lin HC, Tew TB, Hsieh YT, Lin SY, Chang HW, Hu FR, et al. Using optical coherence tomography to assess the role of age and region in corneal epithelium and palisades of vogt. Medicine 2016;95:e4234. http://dx.doi.org/10.1097/MD.0000000000004234.

[39] Lathrop K, Gupta D, Kagemann L, Schuman J, Sundarraj N. Optical coherence tomography as a rapid, accurate, noncontact method of visualizing the palisades of Vogt. Invest Ophthalmol Vis Sci 2012;53(3):1381–7. http://dx.doi.org/10.1167/iovs.11-8524.

[40] Pashtaev NP, Pozdeeva NA, Voskresenskaya AA, Gagloev BV, Shipunov AA. Comparative analysis of the value of information provided by anterior segment optical coherence tomography and confocal laser scanning microscopy for identifying the palisades of Vogt in normal limbus. Vestn Oftalmol 2017;133:60–9. http://dx.doi.org/10.17116/oftalma2017133160-69.

[41] Sigal IA, Steele J, Drexler S, Lathrop KL. Identifying the palisades of Vogt in human ex vivo tissue. Ocul Surf 2016;14:435–9. http://dx.doi.org/10.1016/j.jtos.2016.07.003.

[42] Goldberg MF, Bron AJ. Limbal palisades of Vogt. Trans Am Ophthalmol Soc 1982;80:155–71.